PCCP

Accepted Manuscript

ROYAL SOCIETY OF CHEMISTRY

www.rsc.org/pccp

Theoretical Study of Exciton Dissociation through Hot States at Donor–Acceptor Interface in Organic Photocell

Tomomi Shimazaki and Takahito Nakajima

RIKEN, Advanced Institute for Computational Science

7-1-26 Minatojima-minami-machi, Chuo-ku, Kobe, Hyogo 650-0047, Japan

ABSTRACT

We theoretically study the dissociation of geminate electron-hole pairs (i.e., excitons) through vibrational hot states at the donor–acceptor interface of organic photocells. To conduct this, we modify the formalism of Rubel et al. [Phys. Rev. Lett., **100**, 196602 (2008)], and use the theoretical concepts of Arkhipov et al. [Phys. Rev. Lett., **82**, 1321 (1999)] and Knights et al. [J. Phys. Chem. Sol., **35**, 543 (1974)] to consider vibrational hot states. The effects of band-offset energy and the dissipation of excess energy are discussed on the basis of calculations of the escape probability for hot electrons. Furthermore, we show that vibrational hot state and delocalization of excitons lead to an increased probability to separate geminate electron-hole pairs.

I. INTRODUCTION

Organic photocells based on π-conjugated oligomers and polymers have attracted significant attention as sources of natural renewable power.[1-13] The cost of producing organic solar cells is less than that of conventional solar cells, partly because manufacturing organic semiconductors does not require high-temperature processing, unlike inorganic semiconductors such as poly- and amorphous-silicon materials. Additionally, organic semiconductors offer unique features: they are easily functionalized, allowing them to be targeted for a myriad of applications; they can be produced as thin flexible films; and they can be easily processed. These features make them attractive from both scientific and industrial viewpoints. However, at present, the energy conversion efficiencies of organic photocells remain low compared with those of inorganic photocells.[3] To improve the efficiency of organic photocells, the mechanisms of photocurrent generation in organic semiconductors have been actively investigated. The dissociation of electron-hole pairs (i.e., excitons) generated by the absorption of a photon is a key step in generating photocurrent. In organic semiconductors, which have low dielectric constants, the typical Coulomb binding energy of an exciton at a donor–acceptor heterojunction is a few hundred millielectronvolts,[3, 9, 14, 15] which is considerably greater than the ambient thermal energy of approximately 0.025 eV. Several mechanisms have been proposed to explain the efficient separation of strongly bound electron-hole pairs, such as interfacial electric fields, doping or charge defects, contributions from entropy effects, and structural heterogeneity.[16-24] In this paper, we focus on "hot" charge-transfer (CT) states at the donor–acceptor junctions of organic photocells.[3] Figure 1 shows a schematic of how hot CT states are generated.[3, 4] An exciton is created by absorbing a photon in the donor region of the solar cell, following

which the exciton diffuses to the donor–acceptor interface. Subsequently, the electron transfers to the acceptor region, where the interface has a band-offset energy because of the difference between the energy of the lowest unoccupied molecular orbital (LUMO) of the donor and acceptor molecules. Thus, the initial CT state immediately after electron transfer is hot compared with the thermally relaxed states to which the electron can decay by dissipating its excess energy. Several groups have reported evidence of a hot CT state, and both experimental and theoretical studies have indicated its importance in the dissociation process of geminate electron-hole pairs.[3-5, 7, 25-32] In this paper, we theoretically analyze the exciton-dissociation process through the hot CT state.

To describe exciton dissociation, Rubel et al. proposed a theoretical methodology based on the Miller–Abrahams transition rate and the rate equations involving particle densities.[33, 34] They gave an analytical expression for the exciton dissociation probability and proved that, in certain limits, their formalism reduces to the Onsager and Frenkel theories. In the method of Rubel et al., the electric field is considered as a force driving charge separation. In the present study, we consider the hot CT state that are involved in exciton dissociation; therefore, we modify the method of Rubel et al. using Arkhipov's theoretical assumption to take into account the excess energy of hot electron.[35, 36] A similar physical concept has been proposed by Knights and Davis for thermally assisted electron-hole pair dissociation, which was adopted for the inorganic amorphous material of selenium.[37] In this paper, we theoretically discuss the effects of the band-offset energy at the donor–acceptor heterojunction and the dissipation of the excess energy resulting from charge separation as the electron relaxes through the hot state.

II. THEORY

We begin by discussing the model, which is schematically depicted in Fig. 2. On the basis of this figure, the dynamics of the particle density in hot states is described as follows:

$$\frac{\partial f_1^h}{\partial t} = -\frac{f_1^h}{\tau_h} - \frac{f_1^h}{\tau_{h\to 0}} - a_1^h f_1^h + a_1^h b_1^h f_2^h + g\,, \tag{1.1}$$

$$\frac{\partial f_i^h}{\partial t} = -\frac{f_i^h}{\tau_h} + a_{i-1}^h f_{i-1}^h + \left(-a_i^h - a_{i-1}^h b_{i-1}^h\right) f_i^h + a_i^h b_i^h f_{i+1}^h\,, \tag{1.2}$$

$$\frac{\partial f_n^h}{\partial t} = -\frac{f_n^h}{\tau_h} + a_{n-1}^h f_{n-1}^h + \left(-a_n^h - a_{n-1}^h b_{n-1}^h\right) f_n^h\,, \tag{1.3}$$

where f_i^h is the hot-state particle density at site i, a_i^h is the forward-transition rate from site i to site $i+1$, and $a_i^h b_i^h$ is the backward-transition rate from site $i+1$ to site i. Explicit expressions for a_i^h and b_i^h are presented later. The hot-state particle density of site 1 decreases at the rate $\tau_{h\to 0}^{-1}$ by the recombination of hot electrons with holes. Furthermore, hot particles transition to the ground state at the rate of τ_h^{-1}. Conversely, hot particles with excess energy $\langle E_h \rangle$ are injected at rate g into the hot state at site 1, as described by Eq. (1.1). The particle density in the thermally relaxed state is obtained from the following rate equations:

$$\frac{\partial f_1}{\partial t} = -a_1 f_1 - \frac{f_1}{\tau_{r\to 0}} + a_1 b_1 f_2 + \frac{f_1^h}{\tau_h}\,, \tag{2.1}$$

$$\frac{\partial f_i}{\partial t} = a_{i-1} f_{i-1} + \left(-a_i - a_{i-1} b_{i-1}\right) f_i + a_i b_i f_{i+1} + \frac{f_i^h}{\tau_h}\,, \tag{2.2}$$

$$\frac{\partial f_n}{\partial t} = a_{n-1} f_{n-1} + \left(-a_n - a_{n-1} b_{n-1}\right) f_n + \frac{f_n^h}{\tau_h}\,, \tag{2.3}$$

where f_i is the relaxed-state particle density at site i, and a_i and $a_i b_i$ are the forward- and backward-transition rates, respectively. The particle density f_1 decreases at the rate $\tau_{r\to 0}^{-1}$ by the recombination of thermally relaxed electron-hole pairs. Conversely, the particle density f_i increase at the rate f_i^h/τ_h. In this study, we only consider stable static states; therefore, the conditions $\partial f_i/\partial t = 0$ and $\partial f_i^h/\partial t = 0$ are imposed in Eqs. (1) and (2), leading to the following matrix representation for Eqs. (1) and (2):

$$\begin{pmatrix} \mathbf{B}_h & 0 \\ \boldsymbol{\tau}_h^{-1} & \mathbf{A} \end{pmatrix} \begin{pmatrix} \mathbf{f}^h \\ \mathbf{f} \end{pmatrix} = -\begin{pmatrix} \mathbf{g} \\ \mathbf{0} \end{pmatrix}, \tag{3.1}$$

$$\mathbf{A} = \begin{pmatrix} -a_1 - \tau_{r\to 0}^{-1} & a_1 b_1 & & & \mathbf{0} \\ & \ddots & & & \\ & a_{i-1} & -a_i - a_{i-1} b_{i-1} & a_i b_i & \\ & & & \ddots & \\ \mathbf{0} & & & a_{n-1} & -a_n - a_{n-1} b_{n-1} \end{pmatrix}, \tag{3.2}$$

$$\mathbf{B}_h = \begin{pmatrix} -a_1^h - \tau_h^{-1} - \tau_{h\to 0}^{-1} & a_1^h b_1^h & & & \mathbf{0} \\ & \ddots & & & \\ & a_{i-1}^h & -a_i^h - a_{i-1}^h b_{i-1}^h - \tau_h^{-1} & a_i^h b_i^h & \\ & & & \ddots & \\ \mathbf{0} & & & a_{n-1}^h & -a_n^h - a_{n-1}^h b_{n-1}^h - \tau_h^{-1} \end{pmatrix}, \tag{3.3}$$

$$\boldsymbol{\tau}_h^{-1} = \begin{pmatrix} \tau_h^{-1} & & \mathbf{0} \\ & \ddots & \\ \mathbf{0} & & \tau_h^{-1} \end{pmatrix}, \tag{3.4}$$

where $\mathbf{f} = \begin{pmatrix} f_1 & \cdots & f_n \end{pmatrix}^T$, $\mathbf{f}^h = \begin{pmatrix} f_1^h & \cdots & f_n^h \end{pmatrix}^T$, and $\mathbf{g} = \begin{pmatrix} g & 0 & \cdots & 0 \end{pmatrix}^T$. The particle densities in both hot and relaxed states are obtained as follows:

$$\mathbf{f}^h = -\mathbf{B}_h^{-1}\mathbf{g} = -g\begin{pmatrix} \left[\mathbf{B}_h^{-1}\right]_{11} \\ \left[\mathbf{B}_h^{-1}\right]_{21} \\ \vdots \\ \left[\mathbf{B}_h^{-1}\right]_{n1} \end{pmatrix}, \tag{4.1}$$

$$\mathbf{f} = -\mathbf{A}^{-1}\boldsymbol{\tau}_h^{-1}\mathbf{f}^h = \tau_h^{-1} g\begin{pmatrix} \sum_{s=1}^{n}\left[\mathbf{A}^{-1}\right]_{1s}\left[\mathbf{B}_h^{-1}\right]_{s1} \\ \sum_{s=1}^{n}\left[\mathbf{A}^{-1}\right]_{2s}\left[\mathbf{B}_h^{-1}\right]_{s1} \\ \vdots \\ \sum_{s=1}^{n}\left[\mathbf{A}^{-1}\right]_{ns}\left[\mathbf{B}_h^{-1}\right]_{s1} \end{pmatrix}. \tag{4.2}$$

The escape probability η and the recombination probability θ are obtained from

$$\eta = \frac{a_n f_n}{g} + \frac{a_n^h f_n^h}{g} \equiv \eta_r + \eta_h, \tag{5.1}$$

$$\theta = \frac{f_1}{\tau_{r\to 0} g} + \frac{f_1^h}{\tau_{h\to 0} g} \equiv \theta_r + \theta_h, \tag{5.2}$$

$$\eta + \theta = 1, \tag{5.3}$$

where $\eta_{r(h)}$ and $\theta_{r(h)}$ represent the partial contributions of the escape and recombination probabilities for the relaxed and hot states, respectively. From Eqs. (4) and (5), we see that the escape and recombination probabilities are independent of the parameter g. To calculate the escape probability, we use the Miller–Abrahams rate for electron transfer between the relaxed states:[33, 38]

$$a_i = \begin{cases} a_0 \exp\left(-\dfrac{E_{i+1} - E_i}{k_B T}\right) & \text{if} \quad E_{i+1} > E_i \\ a_0 \quad \text{if} \quad E_{i+1} \le E_i, \end{cases} \tag{6.1}$$

$$b_i = \exp\left(\frac{E_{i+1} - E_i}{k_B T}\right), \tag{6.2}$$

where a_0 is a constant related to quantum tunneling, k_B is the Boltzmann constant, T is the temperature, and E_i is the energy of site i. The explicit expression for E_i

is given in the following section. Next, to describe the hot states, we use the theoretical concept of Arkhipov et al. whereby hot excitons (bound electron-hole pairs) are assumed to be surrounded by a vibrational bath that absorbs the excess energy.[35, 36] Knights et al. have also proposed the thermally assisted free-carrier generation process in inorganic material.[37] If a band-offset energy E_{offset} exists between the donor and acceptor LUMO levels at the donor–acceptor interface of the photocell (as shown in Fig. 1), electrons injected from the acceptor side have excess energy comparable with the band-offset energy. Thus, we consider hot electrons to be situated in a vibrational bath and to have excess energy $\langle E_h \rangle = E_{\text{offset}}$. Here, we assume that the dissipations of excess energy occur on-site, as seen in Fig. 2, because the vibrational hot states are considered as local phenomena. These considerations lead to the following rates with the local temperature of $E_{\text{offset}} + k_B T$ for hot states:

$$a_i^h = \begin{cases} a_0 \exp\left(-\dfrac{E_{i+1} - E_i}{E_{\text{offset}} + k_B T} \right) & \text{if} \quad E_{i+1} > E_i \\ a_0 \quad \text{if} \quad E_{i+1} \le E_i, \end{cases} \tag{7.1}$$

$$b_i^h = \exp\left(\frac{E_{i+1} - E_i}{E_{\text{offset}} + k_B T} \right). \tag{7.2}$$

We can obtain analytical expressions for the matrix elements of $\mathbf{A}^{-1}$ by inverting the tridiagonal matrix (see Appendix):

$$\left[\mathbf{A}^{-1} \right]_{1s} = -\frac{\displaystyle\sum_{j=s}^{n} \frac{1}{a_j} \exp\left(\frac{E_j - E_1}{k_B T} \right)}{1 + \tau_{r\to 0}^{-1} \displaystyle\sum_{j=1}^{n} \frac{1}{a_j} \exp\left(\frac{E_j - E_1}{k_B T} \right)}, \tag{8.1}$$

$$\left[\mathbf{A}^{-1}\right]_{ns} = -\frac{1}{a_n}\frac{1+\tau_{r\to 0}^{-1}\sum_{j=1}^{s-1}\frac{1}{a_j}\exp\left(\frac{E_j-E_1}{k_BT}\right)}{1+\tau_{r\to 0}^{-1}\sum_{j=1}^{n}\frac{1}{a_j}\exp\left(\frac{E_j-E_1}{k_BT}\right)}. \tag{8.2}$$

The escape probability is described using Eqs. (5.1) and (8.2) as follows:

$$\eta = \eta_r + \eta_h, \tag{9.1}$$

$$\eta_r = \sum_{s=1}^{n}\frac{1+\tau_{r\to 0}^{-1}\sum_{j=1}^{s-1}\frac{1}{a_j}\exp\left(\frac{E_j-E_1}{k_BT}\right)}{1+\tau_{r\to 0}^{-1}\sum_{j=1}^{n}\frac{1}{a_j}\exp\left(\frac{E_j-E_1}{k_BT}\right)}\left(-\frac{\left[\mathbf{B}_h^{-1}\right]_{s1}}{\tau_h}\right), \tag{9.2}$$

$$\eta_h = -a_n^h\left[\mathbf{B}_h^{-1}\right]_{n1}, \tag{9.3}$$

where η_r and η_h are the partial contributions of the escape probability η for the relaxed and hot states, respectively. The recombination probability θ is similarly obtained from Eqs. (5.2) and (8.1) as follows:

$$\theta = \theta_r + \theta_h, \tag{10.1}$$

$$\theta_r = \sum_{s=1}^{n}\frac{\sum_{j=s}^{n}\frac{1}{a_j}\exp\left(\frac{E_j-E_1}{k_BT}\right)}{\tau_{r\to 0}+\sum_{j=1}^{n}\frac{1}{a_j}\exp\left(\frac{E_j-E_1}{k_BT}\right)}\left(-\frac{\left[\mathbf{B}_h^{-1}\right]_{s1}}{\tau_h}\right), \tag{10.2}$$

$$\theta_h = -\frac{\left[\mathbf{B}_h^{-1}\right]_{11}}{\tau_{h\to 0}}, \tag{10.3}$$

where θ_r (θ_h) is the partial contribution of the recombination probability for the relaxed (hot) state.

We now compare Eq. (10.2) with the following recombination probability derived by Rubel et al.:

$$\theta_{\text{Rubel}} = \frac{\sum_{j=1}^{n} \exp\left(\frac{E_j - E_1}{k_B T}\right)}{\tau_{r\to 0} + \sum_{j=1}^{n} \exp\left(\frac{E_j - E_1}{k_B T}\right)}. \tag{11}$$

Equation (10.2) reduces to Rubel's expression (11) in the single-state model without hot states. Therefore, Eq. (10.2) is similar Eq. (11) but accounts for the hot states. From Eq. (4.1), the hot-state particle density of site s is $-\left[\mathbf{B}_h^{-1}\right]_{s1} g$; therefore, the particle generation rate is proportional to $-\left[\mathbf{B}_h^{-1}\right]_{s1}/\tau_h$, where τ_h is the relaxation time for particles that relax from the hot state to the relaxed state. Thus, because the model depicted in Fig. 2 accounts for relaxation from every site, Eq. (10.2) contains all contributions from the hot states. Note also that Onsager and Frenkel theories often constitute a starting point for discussing the dissociation efficiency of geminate electron-hole pairs.[39-43] Rubel et al. showed that η_{Ruble}, which is obtained from $\eta_{\text{Rubel}} = 1 - \theta_{\text{Rubel}}$, reduces to the Onsager and Frenkel expressions in some limiting cases,[33] which indicates that the escape probability given by Eq. (9) also reduces to these same expressions from Onsager and Frenkel.

III. CALCULATIONS AND DISCUSSIONS

In this section, we present results calculated using the model described in Sec. II. The following Coulomb potential with the dielectric constant ε_s is employed to obtain the energy level E_i for site i:

$$E_i = -\frac{1}{4\pi\varepsilon_0\varepsilon_s}\frac{1}{|\mathbf{R}_i|}. \quad (i = 1, 2, \text{K}, n) \tag{15}$$

Here, ε_0 is the vacuum permittivity, and $\mathbf{R}_i$ gives the position of site i. In this study, to focus on the effects of the hot states, we consider the case of no external electric field. We use an initial separation distance of 8.5 Å for the electron-hole pair, and the distance between neighboring sites is 10 Å. We use 30 sites, which is sufficient to completely separate the electron-hole pairs in a material with a dielectric constant of $\varepsilon_s = 3.0$ and at room temperature ($T = 300$ K). Additionally, we use $\tau_{r\to 0} = 100$ ps, $\tau_{h\to 0} = 100$ ps, and $a_0^{-1} = 10$ fs for the parameters of the simulation. To begin, we show the escape probabilities in Fig. 3 as a function of band-offset energy E_{offset} and dissipation time τ_h. In Fig. 3, the vertical axes denote the offset energy, and the horizontal axes denote the dissipation time. The probability is denoted by color: red (blue) indicates high (low) escape probability for hot electrons. Figure 3(a) shows that larger band-offset energies and longer dissipation times yield higher escape probabilities; however, the band-offset energy seems to more strongly influence the disassociation of electron-hole pairs than does the dissipation time. Even if a system has long dissipation times, the escape probabilities are low in the case of small band-offset energy. Higher band-offset energies are required to overcome the strong binding energy of excitons in organic semiconductors, which have low dielectric constants. Furthermore, we show the results for η_r and η_h in Figs. 3(b) and 3(c), respectively, where η_r (η_h) represents the contribution to the escape probability from relaxed (hot) states. In Fig. 3(b), η_r is significantly low for all band-offset energies and dissipation times considered. Conversely, the results shown in Figs. 3(a) and 3(c) are similar, which suggests that the dissociation of a geminate electron-hole pair occurs through the hot states. For example, for a band-offset energy of 0.35 eV and a dissipation time of 2.0 ps, we obtain an escape

probability of 0.242, where the contributions from the relaxed and hot states are 0.068 and 0.174, respectively. Thus, the hot states serve as a path for the separation process of excitons.

We discuss how delocalization affects the charge-separation process.[30, 44] In Eq. (15), electrons and holes are represented by point charges; however, in organic semiconductors, they are delocalized to degrees that depend on their local environment. To consider the delocalization effect, we use the following energy-level model:

$$E_i = -\frac{1}{4\pi\varepsilon_0\varepsilon_s}\int \frac{\left|\phi_{\mathrm{HOMO}}(\mathbf{r})\right|^2}{\left|\mathbf{r}-\mathbf{R}_i\right|}d\mathbf{r}, \quad (i = 1, 2, \mathrm{K}, n) \tag{16}$$

where $\mathbf{r}$ is the position of the delocalized hole in an oligomer (molecule). $\mathbf{R}_i$ is the position of site i, which is perpendicularly located against the π-conjugation plane on the center of the oligomer. This paper assumes that electron is localized on the sites for simplicity, and therefore the positon of electron can be described by $\mathbf{R}_i$. $\phi_{\mathrm{HOMO}}(\mathbf{r})$ is the wave function of the highest occupied molecular orbital (HOMO) of the oligomer. Here, we employ methyl-thiophene hexamer described in the inset of Fig. 4(a). The HOMO orbital is obtained by the HF/6-31G* quantum chemistry technique. We execute the numerical integrations on $\mathbf{r}$ over the whole space to calculate Eq. (16), because of the assumption that hole is delocalized over the HOMO orbital. The recursive computation technique based on Gaussian-basis set is employed for the estimations.[45] The energy levels obtained from Eq. (16) are shown by black circles in Fig. 4(a) and, for comparison, the energy levels calculated using Eq. (15) are shown by open circles. The escape probabilities obtained from Eqs. (15) and (16) are shown by the dashed and solid lines in Fig. 4(b), respectively, as a function of band-offset energies. For these

calculations, we use an energy-dissipation time of 2.0 ps, with the other parameters being the same as those used to produce Fig. 3. Figure 4(b) allows us to confirm that, for all band-offset energies, the delocalization effect leads to a larger escape probability compared with the results of Eq. (15). The binding energies at the initial separation distance are 0.56 and 0.23 eV for the localized and delocalized models, respectively. The smaller binding energy given by the delocalized model gives larger escape probabilities. The energy difference between the first and second sites (i.e., $E_2 - E_1$) further influences the escape process. These energy differences are 0.31 and 0.11 eV for the localized and delocalized models, respectively. Equation (15) gives a larger energy difference, as observed in Fig. 4(a), which inhibits electrons from moving away from the donor–acceptor interface by a random-walk process. Thus, the localization of holes reduces the escape probability of hot electrons, whereas the delocalization of holes enhances the exciton dissociation process.

We now briefly discuss the choice of parameters in this study. The band-offset energy depends on the combination of donor–acceptor materials used in organic photocells. In many cases, the band-offset energies are approximately 0.3–0.4 eV.[1, 3, 46-48] Thus, we adopt herein the band-offset energy of 0.35 eV to obtain Fig. 4. However, experimentally observing the energy-dissipation time is difficult because of short-lived hot CT states; nevertheless, some groups report lifetimes of 1.0 to 3.0 ps.[7, 49, 50] We thus use the energy-dissipation time of 2.0 ps to obtain the results. Conversely, typical exciton lifetimes and recombination times of electron-hole pairs are in the range from about 50 ps to 1 ns,[3, 51] so we employ 100 ps for the $\tau_{r\to 0}$ and $\tau_{h\to 0}$ parameters. The distance between neighboring sites are determined from the crystalline structure of fullerene derivatives.[52] On the other hand, to accurately estimate the a_0 parameter, we

need to deeply understand the mechanism of electron conduction in organic material. However, at present, fullerene derivatives, which are frequently used for electron acceptor organic materials, are actively investigated to make clear the electron conduction mechanism.[52-55] Recent studies suggest the inapplicability of Marcus-like electron-hopping model for the electron transport in fullerene derivatives, and other mechanisms have been proposed.[52, 53, 56-58] We will discuss this mater somewhere.

Finally, we compare our results with those of various theoretical studies that focused on the charge-separation process via hot CT states. Peumans et al. used kinetic Monte Carlo simulations to determine the probability for geminate electron-hole pairs to separate at a donor–acceptor interface.[16] In their simulations, hot electrons with excess energy were injected across a donor–acceptor interface, and the results indicated high carrier-collection efficiencies. Tamura et al. combined first-principles electronic-structure calculations and a quantum dynamical analysis to study the exciton-dissociation process.[30] They reported that the delocalization of charges and the vibronically hot nature of the CT state both promote the charge-separation process to a point where it overcomes the strong Coulomb attraction within geminate electron-hole pairs. In the present study, we also showed the importance of the delocalization effect and the hot CT states, and the results of our calculations support these conclusions.

IV. SUMMARY

In this paper, we discuss the charge-separation process through the hot CT state. To conduct this, we modify the method of Rubel et al. and employ the theoretical concepts of Arkhipov et al. and Knights et al. to describe the hot state. We begin by showing how

the band-offset energy and the dissipation time of the excess energy affect the charge-separation process. This is done by calculating the escape probabilities for hot electrons and demonstrating that the charge-separation process proceeds mainly through the hot states. In addition, we show that the delocalization of hole can significantly raise the escape probability of hot excitons, because the initial binding energy of the electron-hole pair decreases and the hot electron undergoes a prompt random walk.

APPENDIX

We show here a brief derivation of Eqs. (8.1) and (8.2). First, we consider the tridiagonal matrix C_n:

$$\mathbf{C}_n = \begin{pmatrix} v_1 & w_1 & & & & \\ u_1 & v_2 & w_2 & & & \\ & u_2 & v_3 & w_3 & & \\ & & \ddots & \ddots & \ddots & \\ & & & u_{n-2} & v_{n-1} & w_{n-1} \\ & & & & u_{n-1} & v_n \end{pmatrix}. \tag{A1}$$

The inverted tridiagonal matrix is obtained analytically as follows:[59-61]

$$\left[\mathbf{C}_n^{-1}\right]_{ij} = \begin{cases} (-1)^{i+j}\left[\prod_{s=i}^{j-1} w_s\right]\Theta_{i-1}\Phi_{j+1}/\Theta_n\,, & i<j \\ \Theta_{i-1}\Phi_{i+1}/\Theta_n\,, & i=j \\ (-1)^{i+j}\left[\prod_{s=j}^{i-1} u_s\right]\Theta_{j-1}\Phi_{i+1}/\Theta_n\,, & i>j, \end{cases} \tag{A2}$$

where Θ_i and Φ_i are defined as

$$\Theta_i = v_i\Theta_{i-1} - u_{i-1}w_{i-1}\Theta_{i-2}, \tag{A3}$$

$$\Phi_i = v_i \Phi_{i+1} - u_i w_i \Phi_{i+2} . \tag{A4}$$

Here, $\Theta_1 = v_1$, $\Theta_0 = 1$, $\Phi_n = v_n$, and $\Phi_{n+1} = 1$. For the matrix $\mathbf{A}$ of Eq. (3.2), Θ_s and Φ_s are expressed as

$$\Theta_s = (-1)^s \prod_{j=1}^{s} a_j \left[1 + \tau_0^{-1} \sum_{j=1}^{s} \frac{1}{a_j} \exp\left(\frac{E_j - E_1}{k_B T} \right) \right], \tag{A5}$$

$$\Phi_s = -(-1)^{n-s} \prod_{j=s}^{n} a_j \left[1 + a_{s-1} \sum_{j=s}^{n} \frac{1}{a_j} \exp\left(\frac{E_j - E_{s-1}}{k_B T} \right) \right]. \tag{A6}$$

The following equations are obtained from Eqs. (A2) and (3.2):

$$\left[\mathbf{A}^{-1} \right]_{1s} = (-1)^{1+s} \prod_{k=1}^{s-1} a_k b_k \frac{\Phi_{s+1}}{\Theta_n} , \tag{A7}$$

$$\left[\mathbf{A}^{-1} \right]_{ns} = (-1)^{n+s} \prod_{k=s}^{n-1} a_k \frac{\Theta_{s-1}}{\Theta_n} . \tag{A8}$$

Equations (8.1) and (8.2) are obtained by substituting eqs. (A5) and (A6) into the above equations.

Figure captions

FIG. 1. Schematic illustration of physical mechanism in organic photocells. An exciton is generated by absorption of a photon, which then diffuses to the donor–acceptor interface. Next, electron transfer occurs to form the hot charge-transfer state, which plays an important role in the subsequent charge-separation process.

FIG. 2. One-dimensional n-hopping sites model with one hot (excited) state. The quantity f_i^h is the hot-state particle density at site i, and f_i is the ground-state particle density at site i. a_i^h is the forward-transition rate from site i to site $i+1$, $a_i^h b_i^h$ is the backward-transition rate from site $i+1$ to site i for hot particle densities. a_i and $a_i b_i$ are the forward- and backward-transition rates for the thermally relaxed-state particle density, respectively. $\tau_{h\to 0}^{-1}$ is the rate at which the hot-state particle density of site 1 decreases because of the recombination of hot electrons with holes, and $\tau_{r\to 0}^{-1}$ is the rate at which the particle density f_1 decreases because of the recombination of thermally relaxed electron-hole pairs.

FIG. 3. (a) Total escape probability. Panels (b) and (c) show the partial contributions of η_r and η_h to the escape probability, reflecting the relaxed and hot states, respectively.

FIG. 4. (a) Coulomb potential energy as a function of site position: site 1 is closest to the donor–acceptor interface; site 30 is farthest away. The results for the localized and delocalized models are indicated by open and solid circles, respectively. Inset shows methyl-thiophene hexamer considered for this study. (b) Comparison of escape probability resulting from localized and delocalized models, which are shown by the dashed and solid lines, respectively.

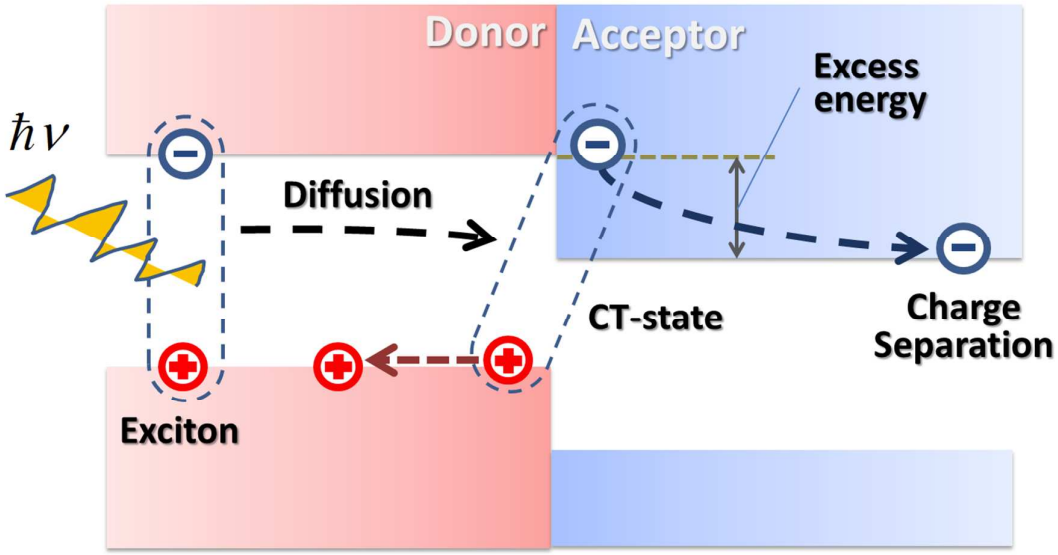

FIG. 1. T. Shimazaki et al.

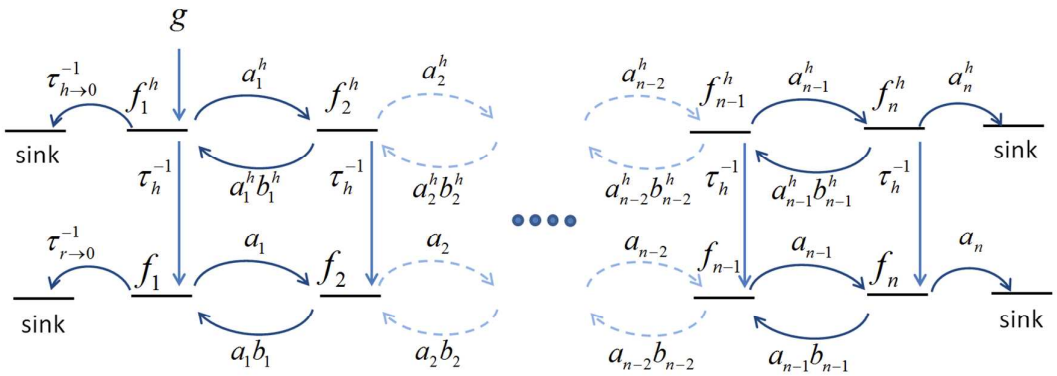

FIG. 2. T. Shimazaki et al.

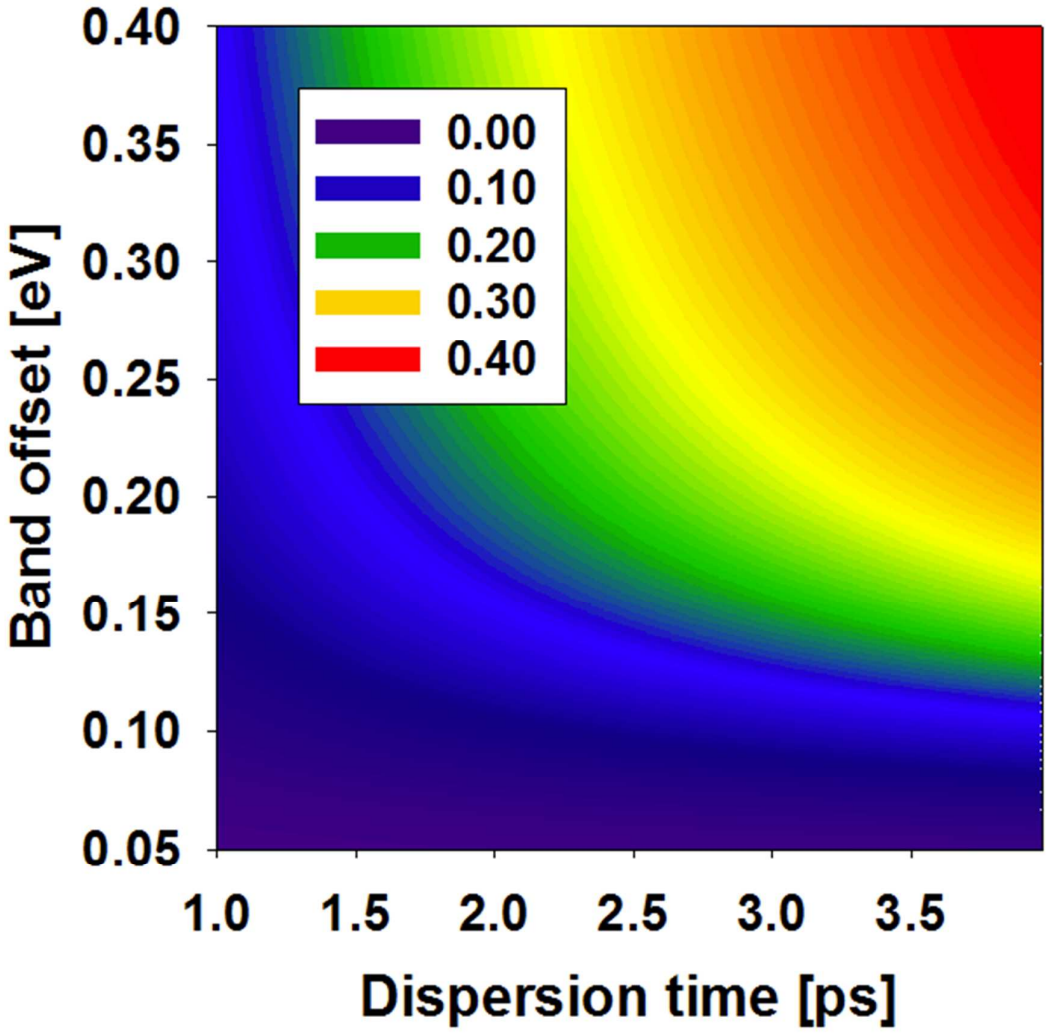

FIG. 3(a). T. Shimazaki et al.

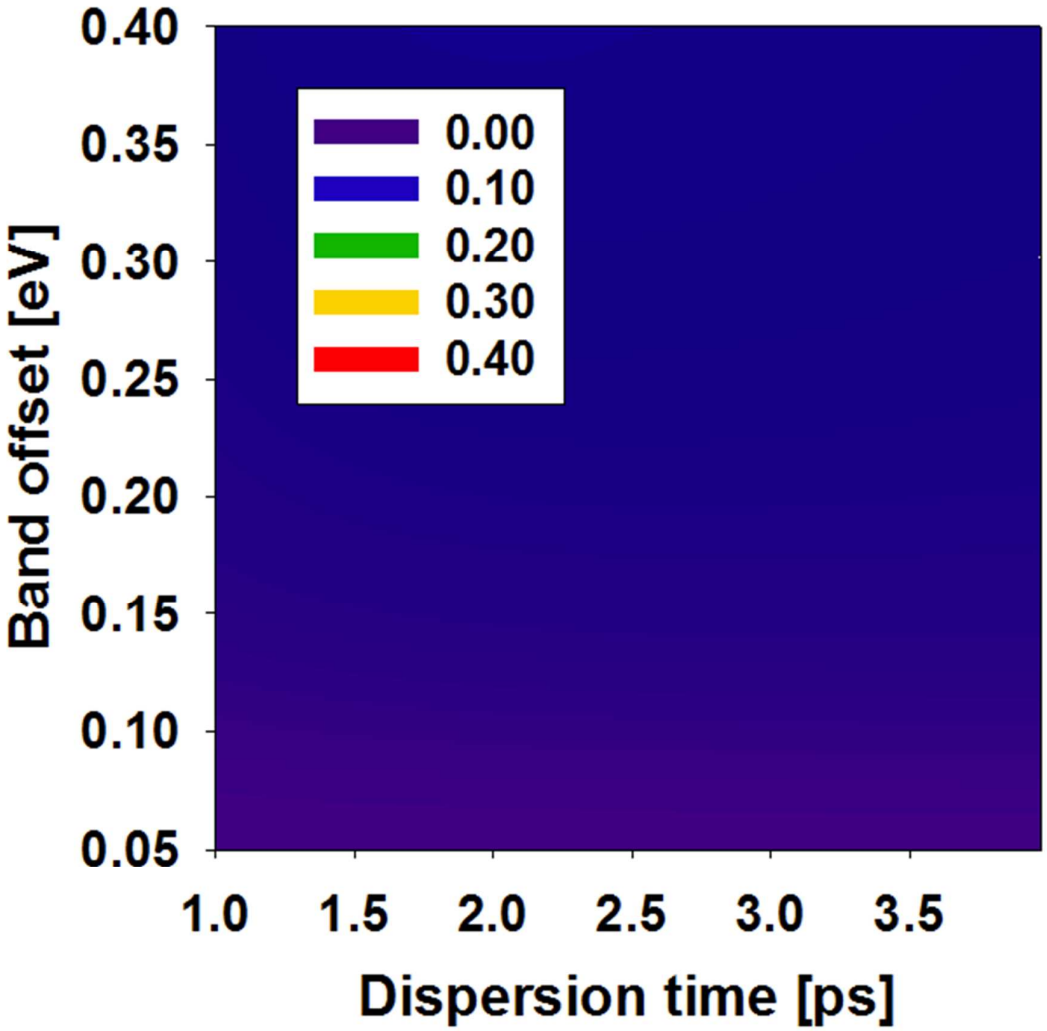

FIG. 3(b). T. Shimazaki et al.

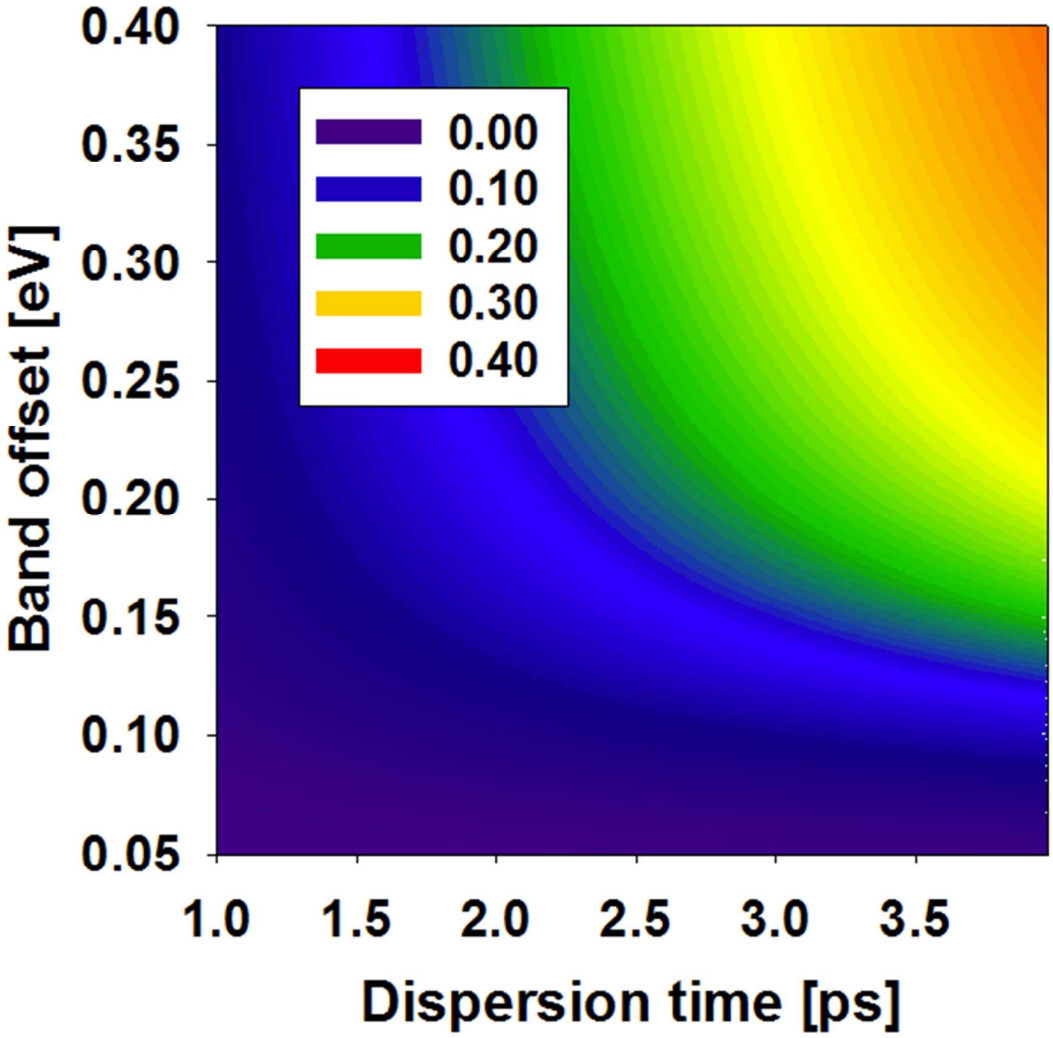

FIG. 3(c). T. Shimazaki et al.

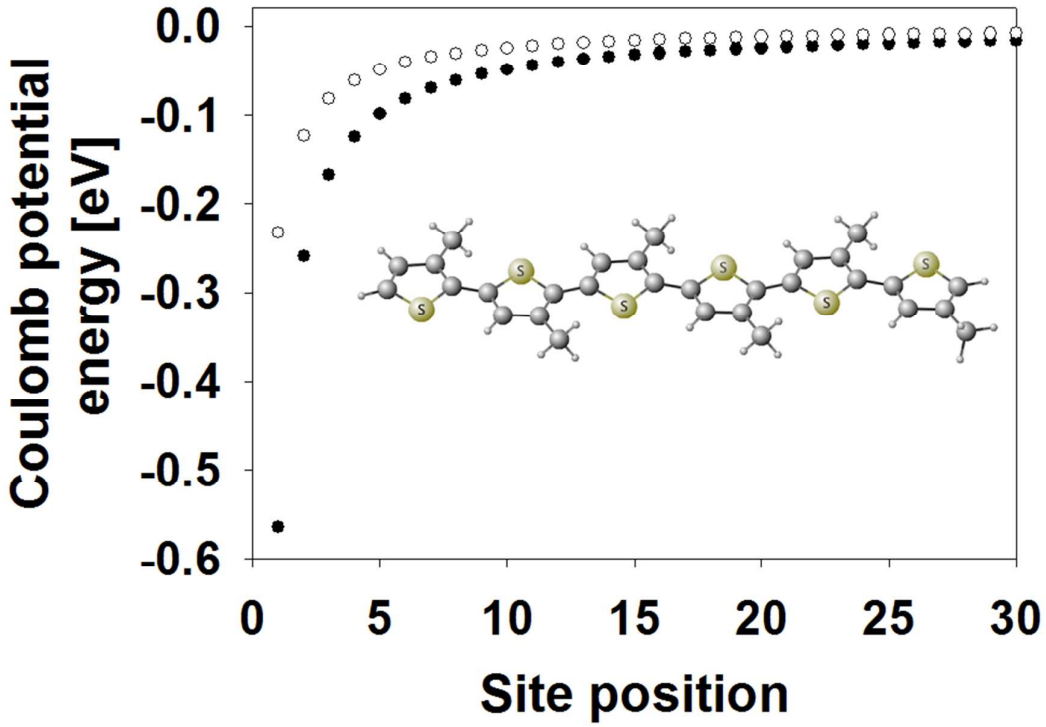

FIG. 4(a). T. Shimazaki et al.

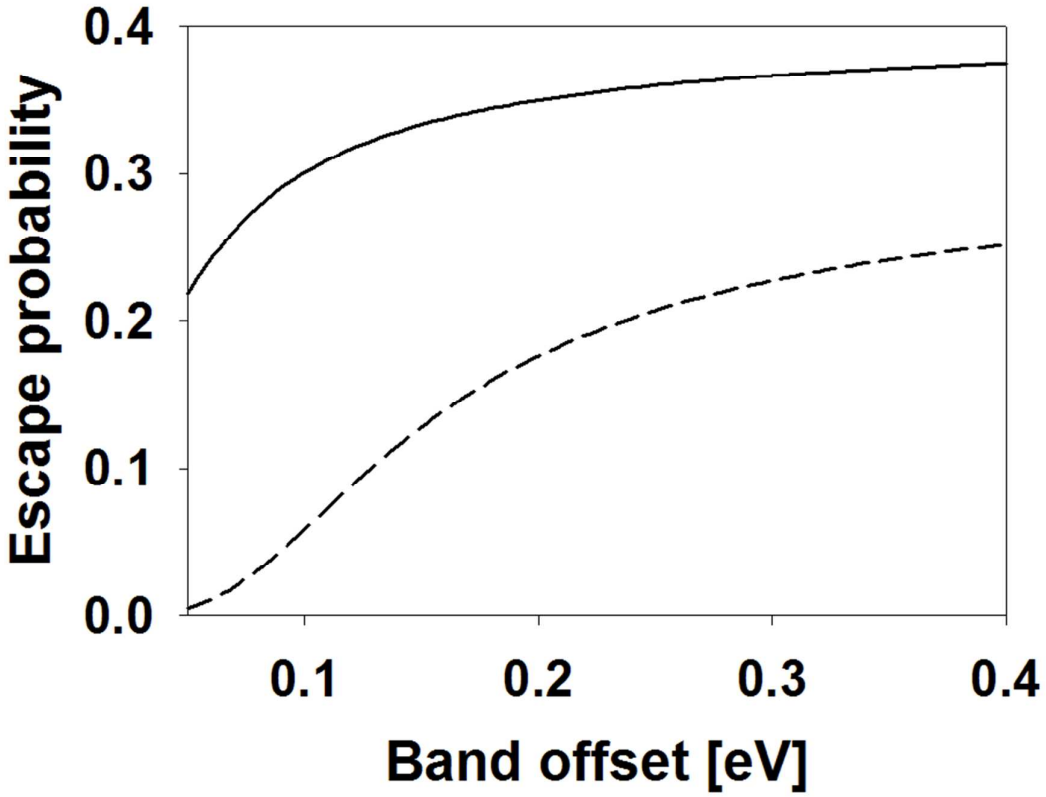

FIG. 4(b). T. Shimazaki et al.

REFERENCES

1. J. L. Bredas, D. Beljonne, V. Coropceanu and J. Cornil, *Chem Rev*, 2004, **104**, 4971-5003.
2. Y. Kanai and J. C. Grossman, *Nano Lett*, 2007, **7**, 1967-1972.
3. T. M. Clarke and J. R. Durrant, *Chem Rev*, 2010, **110**, 6736-6767.
4. A. A. Bakulin, A. Rao, V. G. Pavelyev, P. H. M. van Loosdrecht, M. S. Pshenichnikov, D. Niedzialek, J. Cornil, D. Beljonne and R. H. Friend, *Science*, 2012, **335**, 1340-1344.
5. G. Grancini, M. Maiuri, D. Fazzi, A. Petrozza, H. J. Egelhaaf, D. Brida, G. Cerullo and G. Lanzani, *Nat Mater*, 2013, **12**, 29-33.
6. G. Grancini, M. Binda, L. Criante, S. Perissinotto, M. Maiuri, D. Fazzi, A. Petrozza, H. J. Egelhaaf, D. Brida, G. Cerullo and G. Lanzani, *Nat Mater*, 2013, **12**, 594-595.
7. A. E. Jailaubekov, A. P. Willard, J. R. Tritsch, W. L. Chan, N. Sai, R. Gearba, L. G. Kaake, K. J. Williams, K. Leung, P. J. Rossky and X. Y. Zhu, *Nat Mater*, 2013, **12**, 66-73.
8. O. G. Reid, R. D. Pensack, Y. Song, G. D. Scholes and G. Rumbles, *Chem Mater*, 2014, **26**, 561-575.
9. S. Gelinas, A. Rao, A. Kumar, S. L. Smith, A. W. Chin, J. Clark, T. S. van der Poll, G. C. Bazan and R. H. Friend, *Science*, 2014, **343**, 512-516.
10. F. Gao and O. Inganas, *Phys Chem Chem Phys*, 2014, **16**, 20291-20304.
11. M. L. Jones, R. Dyer, N. Clarke and C. Groves, *Phys Chem Chem Phys*, 2014, **16**, 20310-20320.
12. Y. Tamai, K. Tsuda, H. Ohkita, H. Benten and S. Ito, *Phys Chem Chem Phys*, 2014, **16**, 20338-20346.
13. S. Few, J. M. Frost and J. Nelson, *Phys Chem Chem Phys*, 2015, **17**, 2311-2325.
14. J. L. Bredas, J. E. Norton, J. Cornil and V. Coropceanu, *Accounts Chem Res*, 2009, **42**, 1691-1699.
15. X. Y. Zhu, Q. Yang and M. Muntwiler, *Accounts Chem Res*, 2009, **42**, 1779-1787.
16. P. Peumans and S. R. Forrest, *Chem Phys Lett*, 2004, **398**, 27-31.
17. A. Liu, S. Zhao, S. B. Rim, J. Wu, M. Konemann, P. Erk and P. Peumans, *Adv Mater*, 2008, **20**, 1065-+.
18. B. A. Gregg, *J Phys Chem Lett*, 2011, **2**, 3013-3015.
19. R. G. H. Wilke, G. K. Moghadam, N. H. Lovell, G. J. Suaning and S. Dokos, *J Neural Eng*, 2011, **8**.
20. D. Beljonne, J. Cornil, L. Muccioli, C. Zannoni, J. L. Bredas and F. Castet, *Chem Mater*, 2011, **23**, 591-609.

21. D. P. McMahon, D. L. Cheung and A. Troisi, *J Phys Chem Lett*, 2011, **2**, 2737-2741.
22. W. Chen, T. Xu, F. He, W. Wang, C. Wang, J. Strzalka, Y. Liu, J. G. Wen, D. J. Miller, J. H. Chen, K. L. Hong, L. P. Yu and S. B. Darling, *Nano Lett*, 2011, **11**, 3707-3713.
23. G. Grancini, D. Polli, D. Fazzi, J. Cabanillas-Gonzalez, G. Cerullo and G. Lanzani, *J Phys Chem Lett*, 2011, **2**, 1099-1105.
24. S. R. Yost, L. P. Wang and T. Van Voorhis, *J Phys Chem C*, 2011, **115**, 14431-14436.
25. A. C. Morteani, P. Sreearunothai, L. M. Herz, R. H. Friend and C. Silva, *Phys Rev Lett*, 2004, **92**.
26. J. G. Muller, J. M. Lupton, J. Feldmann, U. Lemmer, M. C. Scharber, N. S. Sariciftci, C. J. Brabec and U. Scherf, *Phys Rev B*, 2005, **72**.
27. H. Ohkita, S. Cook, Y. Astuti, W. Duffy, S. Tierney, W. Zhang, M. Heeney, I. McCulloch, J. Nelson, D. D. C. Bradley and J. R. Durrant, *J Am Chem Soc*, 2008, **130**, 3030-3042.
28. M. Muntwiler, Q. Yang, W. A. Tisdale and X. Y. Zhu, *Phys Rev Lett*, 2008, **101**.
29. S. D. Dimitrov, A. A. Bakulin, C. B. Nielsen, B. C. Schroeder, J. P. Du, H. Bronstein, I. McCulloch, R. H. Friend and J. R. Durrant, *J Am Chem Soc*, 2012, **134**, 18189-18192.
30. H. Tamura and I. Burghardt, *J Am Chem Soc*, 2013, **135**, 16364-16367.
31. H. Tamura and I. Burghardt, *J Phys Chem C*, 2013, **117**, 15020-15025.
32. L. Han, X. X. Zhong, W. Z. Liang and Y. Zhao, *J Chem Phys*, 2014, **140**.
33. O. Rubel, S. D. Baranovskii, W. Stolz and F. Gebhard, *Phys Rev Lett*, 2008, **100**.
34. A. V. Nenashev, S. D. Baranovskii, M. Wiemer, F. Jansson, R. Osterbacka, A. V. Dvurechenskii and F. Gebhard, *Phys Rev B*, 2011, **84**.
35. V. I. Arkhipov, E. V. Emelianova and H. Bassler, *Phys Rev Lett*, 1999, **82**, 1321-1324.
36. V. I. Arkhipov, E. V. Emelianova, S. Barth and H. Bassler, *Phys Rev B*, 2000, **61**, 8207-8214.
37. J. C. Knights and E. A. Davis, *Journal of Physics and Chemistry of Solids*, 1974, **35**, 543.
38. A. Miller and E. Abrahams, *Phys Rev*, 1960, **120**, 745-755.
39. L. Onsager, *J Chem Phys*, 1934, **2**.
40. J. Frenkel, *Phys Rev*, 1938, **54**, 647-648.
41. M. D. Tabak and P. J. Warter, *Phys Rev*, 1968, **173**, 899-&.
42. K. M. Hong and J. Noolandi, *Surf Sci*, 1978, **75**, 561-576.
43. N. Tessler, Y. Preezant, N. Rappaport and Y. Roichman, *Adv Mater*, 2009, **21**, 2741-2761.
44. C. Deibel, T. Strobel and V. Dyakonov, *Phys Rev Lett*, 2009, **103**.

45. S. Obara and A. Saika, *Jouranl of Chemical Physics*, 1986, **84**, 3963.
46. J. J. M. Halls, J. Cornil, D. A. dos Santos, R. Silbey, D. H. Hwang, A. B. Holmes, J. L. Bredas and R. H. Friend, *Phys Rev B*, 1999, **60**, 5721-5727.
47. M. C. Scharber, D. Wuhlbacher, M. Koppe, P. Denk, C. Waldauf, A. J. Heeger and C. L. Brabec, *Adv Mater*, 2006, **18**, 789-+.
48. B. C. Thompson and J. M. J. Frechet, *Angew Chem Int Edit*, 2008, **47**, 58-77.
49. I. G. Scheblykin, A. Yartsev, T. Pullerits, V. Gulbinas and V. Sundstrom, *J Phys Chem B*, 2007, **111**, 6303-6321.
50. J. M. Szarko, B. S. Rolczynski, S. J. Lou, T. Xu, J. Strzalka, T. J. Marks, L. P. Yu and L. X. Chen, *Adv Funct Mater*, 2014, **24**, 10-26.
51. J. Tsutsumi, H. Matsuzaki, N. Kanai, T. Yamada and T. Hasegawa, *J Phys Chem C*, 2013, **117**, 16769-16773.
52. F. Gajdos, H. Oberhofer, M. Dupuis and J. Blumberger, *J Phys Chem Lett*, 2013, **4**, 1012-1017.
53. D. L. Cheung and A. Troisi, *J Phys Chem C*, 2010, **114**, 20479-20488.
54. H. Oberhofer and J. Blumberger, *Phys Chem Chem Phys*, 2012, **14**, 13846-13852.
55. J. Ide, D. Fazzi, M. Casalegno, S. V. Meille and G. Raos, *J Mater Chem C*, 2014, **2**, 7313-7325.
56. J. H. Schon, C. Kloc and B. Batlogg, *Phys Status Solidi B*, 2001, **225**, 209-213.
57. S. Fratini and S. Ciuchi, *Phys Rev Lett*, 2009, **103**.
58. A. Troisi, *Chem Soc Rev*, 2011, **40**, 2347-2358.
59. R. A. Usmani, *Linear Algebra Appl*, 1994, **212**, 413-414.
60. R. A. Usmani, *Comput Math Appl*, 1994, **27**, 59-66.
61. C. M. d. Fonseca, *Jornal of Computational and Applied Mathematics*, 2007, **200**, 283.